

Dilepton production by dynamical quasiparticles in the strongly interacting quark gluon plasma

O. Linnyk*

Institut für Theoretische Physik, Johann Wolfgang Goethe University, 60438 Frankfurt am Main, Germany

(Dated: November 4, 2018)

The dilepton production by the constituents of the strongly interacting quark-gluon-plasma (sQGP) is addressed. In order to make quantitative predictions at realistically low plasma temperatures ($O(T_c)$), experimentally relevant low dilepton mass ($O(1 \text{ GeV})$) and strong coupling ($\alpha_S \sim 0.5 \div 1$), we take into account not only the higher order pQCD reaction mechanisms, but also the non-perturbative spectral functions and self-energies of the quarks, anti-quarks and gluons thus going beyond the leading twist. For this purpose, our calculations utilize parametrizations of the non-perturbative propagators for quarks and gluons provided by the dynamical quasi-particle model (DQPM) matched to reproduce lattice data. The DQPM describes QCD properties in terms of single-particle Green's functions (in the sense of a two-particle irreducible approach) and leads to the notion of the constituents of the sQGP being effective quasiparticles, which are massive and have broad spectral functions (due to large interaction rates). In the present work, we derive the off-shell cross sections of dilepton production in the reactions $q + \bar{q} \rightarrow l^+ l^-$ (Drell-Yan mechanism), $q + \bar{q} \rightarrow g + l^+ l^-$ (quark annihilation with the gluon Bremsstrahlung in the final state), $q(\bar{q}) + g \rightarrow q(\bar{q}) + l^+ l^-$ (gluon Compton scattering), $g \rightarrow q + \bar{q} + l^+ l^-$ and $q(\bar{q}) \rightarrow q(\bar{q}) + g + l^+ l^-$ (virtual gluon decay, virtual quark decay) in the sQGP by dressing the quark and gluon lines in the perturbative diagrams with the DQPM propagators for quarks and gluons.

PACS numbers: 25.75.Nq, 25.75.Cj, 24.85.+p, 12.38.Lg, 13.60.Hb

I. INTRODUCTION

Since many years the transition between the hadronic phase and the quark-gluon plasma (QGP) as well as the nonperturbative properties of QGP motivate a large community and justify large-scale experiments, in which heavy nuclei are collided at relativistic energies in order to achieve the high energy-densities necessary for the transition to the deconfined state of matter. Electromagnetic probes (i.e. dileptons and photons) are powerful tools to explore the early (hot and dense) stage of the heavy-ion collision, since, unaffected by the final state interaction, they carry to the detector information about the conditions and properties of the environment at the time of their production – encoded in their mass and momentum distributions, – thus providing a glimpse deep into the bulk of the strongly interacting matter [1, 2]. In 1978, E. Shuryak proposed to use dilepton as probes of QGP, after the suggestion was made that the dileptons and photon yields reflect the properties of the medium created in hadron-hadron collisions (see the pioneering works [3–7]).

Real and virtual photons, i.e. dileptons, are emitted over the entire space-time evolution of the heavy-ion collision, from the initial nucleon-nucleon collisions through the hot and dense phase and to the hadron decays after freeze-out. This is both a challenge and advantage of electromagnetic probes. Fortunately, lepton pairs possess an additional degree of freedom (the invariant mass Q^2),

which allows to separate different “physics” by observing the dilepton radiation in different mass ranges. The low mass ($Q < 1 \text{ GeV}$) spectrum of dileptons – generated in heavy ion collisions – is dominated by the vector meson decays, the production of lepton pairs of high mass ($Q > 3 \text{ GeV}$) is governed by the perturbative quantum chromodynamics (pQCD), while the dilepton yield in the intermediate mass range ($1 < Q < 3 \text{ GeV}$) is sensitive to the possible formation of a QGP.

Dilepton measurements have possibly provided a sign of the deconfined matter at SPS energies. The NA60 Collaboration [8–10] has recently found that the effective temperature of the dileptons in the intermediate mass range is lower than the T_{eff} of dileptons at lower masses, which are of hadronic origin. This can be explained, if one assumes that the spectrum at the invariant masses above 1 GeV is dominated by the partonic channels in the QGP [11–13]. In this case, the softening of the transverse mass spectrum with growing invariant mass implies that the partonic channels occur dominantly before the collective radial flow has developed. The assumption that the dilepton spectrum at masses above 1 GeV could be dominated by QGP radiation was supported by the studies within the Hadron-String-Dynamics (HSD) transport approach [14], which have shown [15] that the measured dilepton yield at low masses ($Q \leq 1 \text{ GeV}$) can be explained by the dilepton production in the hadron interaction and decay, while there is a discrepancy between the HSD results and the data in the mass range above 1 GeV. This access seen at $Q > 1 \text{ GeV}$ is not accounted for by hadronic sources in HSD – in-medium or free – and might be seen as a signal of partonic matter, manifest already at 158 AGeV incident energy.

*Electronic address: linnyk@fias.uni-frankfurt.de

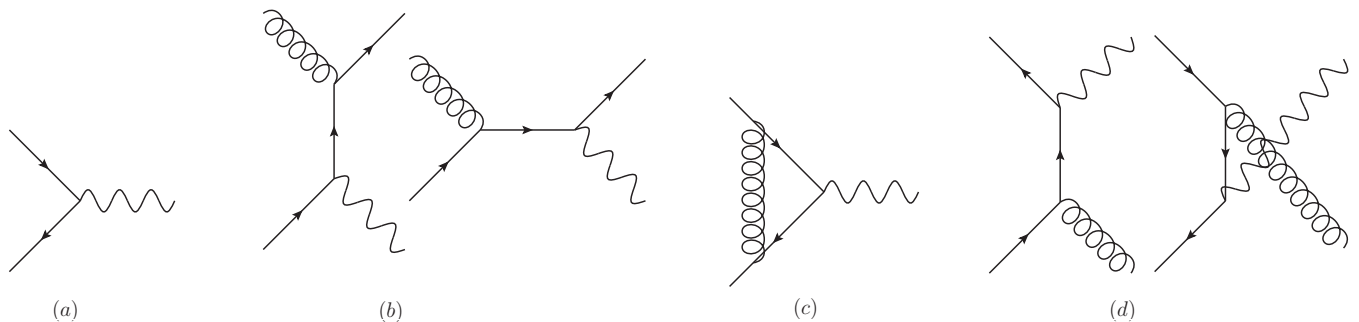


FIG. 1: Perturbative QCD diagrams contributing to the dilepton production up to the order $O(\alpha_S)$: (a) Drell-Yan mechanism, (b) gluon Compton scattering (GCS), (c) vertex correction, (d) quark annihilation with gluon Bremsstrahlung. Virtual photons (wavy lines) split into lepton pairs, spiral lines denote gluons, arrows denote quarks. In each diagram, the time runs from left to right.

Recently, the PHENIX Collaboration has presented first dilepton data from pp and $Au + Au$ collisions at Relativistic-Heavy-Ion-Collider (RHIC) energies of $\sqrt{s} = 200$ GeV [16–19]. The data show an even larger enhancement over hadronic sources in $Au + Au$ reactions in the invariant mass regime from 0.15 to 0.6 GeV, which could not be explained in the scope of the HSD approach neither by meson decays – in-medium or free – nor by hadronic Bremsstrahlung [15]. It is of interest, whether the excess at RHIC is due to the dominance of sources in the QGP [15].

Early predictions of the dilepton emission from QGP relied on perturbative formulae for the cross sections of the virtual photon production in $q + q$ and $q + g$ collisions [4, 20, 21]. Indeed, first concepts of the QGP were guided by the idea of a system of partons which interact weakly, with pQCD cross sections. However, most theoretical estimates of the temperatures, which are reasonably expected to be currently achieved in heavy ion collisions are not extremely large compared to the QCD scale Λ_{QCD} [22]. Therefore, the QCD coupling α_S is not small. In agreement with this early expectation, experimental observations at RHIC indicated that the new medium created in ultra-relativistic Au+Au collisions was interacting strongly - stronger than hadronic matter. Moreover, in line with theoretical studies in Refs. [23–25] the medium showed phenomena of an almost perfect liquid of partons [26–29] as extracted from the strong radial expansion and elliptic flow of hadrons [26–29]. Studies performed in the framework of the lattice regularized QCD [30] have also shown that the high temperature plasma phase is a medium of interacting partons which are strongly screened and influenced by non-perturbative effects even at temperatures as high as $10 T_c$.

Consequently, the concept of perturbatively interacting quarks and gluons as constituents of the QGP had to be given up. Due to large running coupling, the next-to-leading order (NLO) gluon-quark interactions are expected to contribute considerably in addition to the leading order mechanism of quark-quark annihilation ($q\bar{q} \rightarrow$

l^+l^-) to the QGP radiation spectrum. The importance of the higher order corrections is long understood [31]. On the other hand, non-perturbative nature of the sQGP constituents manifests itself not only in their strong coupling, but also in the modified spectral densities and self energies, which should be taken into account in consistent calculations of dilepton production from the QGP.

A cure can be found in reordering perturbation theory: by expanding correlation functions in terms of effective propagators and vertices instead of bare ones [32]. A powerful resummation technique was developed by Braaten, Pisarsky [33] and Wong [34]. The production of dileptons was calculated at leading order in the effective perturbation expansion in [33], using as the effective propagators the bare ones plus one loop corrections evaluated in the high-temperature limit [35–38]. In this approach the singularity of the production cross section – that dominates the dilepton rate – is regularized by the thermal masses of quarks m_{th} and gluons m_g , which are in turn determined by the one-loop leading order result in the thermal perturbation theory (HTL). The approach has been extended to the dilepton radiation from non-equilibrium plasmas in [39, 40].

However, since virtual photon rates need to be evaluated at temperatures that are not very large compared to T_c , it is important to take values for m_{th} , m_g not from the HTL approximation but from, for instance, a fit of the lattice QCD entropy by a gas of massive quarks equation of state [41, 42], as has been done in [43, 44]. Alternatively, one might treat thermal masses in the calculation of the dilepton rates as phenomenological parameters [45].

Not long ago, a first attempt appeared to calculate directly on the lattice the production of dileptons in QGP [46]. The suppression at small Q^2 observed on the lattice has attracted a lot of interest, because it is not what one would expect from (resummed) perturbation theory: The finite thermal masses would indeed produce a drop of the Born (Drell-Yan) term $q + \bar{q} \rightarrow \gamma^*$ because of the threshold effect – as predicted [47] in relation to the

cut-off in the momentum distribution of quarks and confirmed in effective perturbation theory in the works [43–45], – but there are higher order processes ($q\bar{q} \rightarrow \gamma^*g$, $qg \rightarrow \gamma^*q$) that have no threshold and would fill the spectrum at small Q^2 . The effect of multiple scattering of the quark in the plasma (Landau-Pomeranchuk-Migdal effect [48–50]) on the rate of $q\bar{q} \rightarrow \gamma^*$ was considered in the context of the semi-classical approximation in [51], where it was shown that the multiple scatterings lead to the disappearance of the threshold behavior in the Born rate.

In the present work, we pursue a model, in which the (multiple) interaction of quarks and gluon in sQGP is encoded in their effective broad spectral functions. The non-zero width of quarks is related to their strong interaction, which is manifest in the elastic scattering as well as in the virtual gluon emission. By dressing the partonic lines in the dilepton production processes ($q + \bar{q} \rightarrow l^+l^-$, $q + \bar{q} \rightarrow g + l^+l^-$, $q + g \rightarrow q + l^+l^-$) with effective spectral functions we study the effect of the partonic interactions in the plasma on their dilepton radiation, especially in the interesting region of low Q^2 .

The effective propagators were obtained from lattice data in the scope of the Dynamical QuasiParticle Model (DQPM) [52]. DQPM describes QCD properties in terms of single-particle Green’s functions (in the sense of a two-particle irreducible (2PI) approach) and leads a quasi-particle equation of state, which reproduced the QCD equation of state extracted from Lattice QCD calculations. According to the DQPM, the constituents of the sQGP are effective strongly interacting massive partonic quasi-particles with broad spectral functions, i.e. non-vanishing width.

Strong interaction of partons – reflected in their broad widths – leads to higher-twist corrections to the standard pQCD cross sections [53]. The influence of the higher twists is hard to estimate and has been ignored in most calculations so far. Limiting the calculations to the leading twist is a widely used approximation at high energies for the following reason: The higher twists by definition are vanishing in the limit of infinite invariant mass of the lepton pair [54]. Indeed, one observes that by calculating next-to-leading order contributions and refitting the parton distributions accordingly [31, 55], one can already significantly reduce the discrepancy with the data on the double-differential Drell-Yan cross section in elementary $p + p$ collisions [56–58] compared to the LO predictions.

However, the power- Q^2 suppressed (i.e. higher twist) contributions can be large at realistic energies and/or in collective systems with a relatively short interaction length like the sQGP created in heavy-ion collisions. It has been shown [53] that the contribution of higher twists is essential for a proper description of the data on the *triple-differential* Drell-Yan cross section. For instance, quark and gluon off-shellness – arising due to the non-perturbative interaction between the partons – have a large effect on the transverse momentum distribution of produced lepton pairs [53, 59, 60].

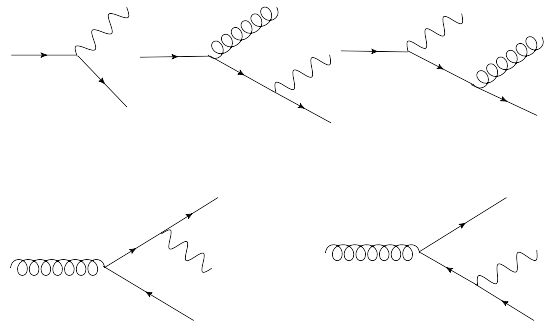


FIG. 2: Diagrams contributing to the dilepton production by virtual quasi-particles in addition to the ones presented in Fig. 1. Upper part: the decay of a virtual quark; Lower part: the decay of a virtual gluon. Virtual photons (wavy lines) split into lepton pairs, spiral lines denote gluons, arrows denote quarks.

In the current paper, we study the dilepton production from dynamical quasi-particle interactions. For this purpose we derive the off-shell cross sections of $q + \bar{q} \rightarrow l^+l^-$, $q + \bar{q} \rightarrow g + l^+l^-$, $q + g \rightarrow q + l^+l^-$ ($\bar{q} + g \rightarrow \bar{q} + l^+l^-$), $q \rightarrow q + g + l^+l^-$ ($\bar{q} \rightarrow \bar{q} + g + l^+l^-$) and $g \rightarrow q + \bar{q} + l^+l^-$ by calculating them for the arbitrary virtualities of external quarks and gluons, while dressing the internal lines with effective self energies, and take into account the non-zero widths of partons by convoluting the obtained cross sections with the effective spectral functions from the DQPM. Using the DQPM parametrizations for the quark(gluon) self-energies, spectral functions and interaction strength, we calculate the dilepton production by partonic interactions in the sQGP while accounting for their non-perturbative dynamics, including the higher twist effects.

The perturbative diagrams for the dilepton production at order up to $O(\alpha_S)$ are illustrated in Fig. 1. Let us briefly summarize the differences of our effective theory approach from the standard pQCD:

- (a) we take into account full off-shell kinematics, in particular the transverse motion and virtuality of the partons,
- (b) quark and gluon lines are dressed with non-perturbative spectral functions and self-energies: the cross sections are derived for arbitrary masses of all external parton lines and integrated over these virtualities weighted with spectral functions (see e.g. Refs [53, 61] for an introduction to the method); the internal lines are dressed with self energies,
- (c) vertices are modified compared to pQCD by replacing the perturbative coupling (that runs with the momentum transfer) with the full running coupling α_S that depends on the temperature T according to lattice data parametrization by [52], while the temperature is related to the local energy

density ϵ by the IQCD equation of state. Note that close to T_c the full coupling increases with the decreasing temperature much faster than the pQCD prediction.

- (d) Due to the broad width for quarks and gluons in the sQGP [43] – which is the consequence of their high interaction rate, – we obtain non-vanishing contributions also from the processes of the decays of virtual quarks ($q \rightarrow q + g + l^+l^-$) and gluons ($g \rightarrow q + \bar{q} + l^+l^-$), which are forbidden kinematically in pQCD (see Fig. 2).

Thus, we utilize the DQPM parametrization for the effective quark and gluon propagator while simultaneously taking into account the NLO reaction mechanisms. This way, we are going in our calculations beyond the leading order in α_S and depart from the leading twist approximation.

The paper is organized as follows. The analysis of the off-shell kinematics and the calculations of the off-shell cross sections in our model are given in section III for each of the partonic processes separately. On the other hand, in the limit of high hard scale Q^2 , the off-shell cross sections should approach the perturbative ones [54, 62]. Therefore, let us first recapitulate the corresponding pQCD results in section II. The off-shell cross sections will be compared to the perturbative ones throughout the section III.

In Section IV we give a simple example of an application of the off-shell cross sections derived above to the calculation of the relative contributions of different processes to the sQGP radiation. We point out, however, that the considerations in the current paper will probably be not detailed enough to be applied to the description of the hot and dense early phase of relativistic heavy-ion collisions, where sQGP is formed. A quantitative comparison to the experimental data and reliable conclusions on the relative contribution of various sources to the experimentally observed thermal dilepton spectrum [8–10, 16–19] requires taking into account the non-equilibrium dynamics of the heavy-ion collision in its full complexity by use of microscopic transport models, which is beyond the scope of this study. The main purpose of the current paper is to built an effective approach for the derivation of the off-shell cross sections for the interaction of dynamical quasi-particles as constituents of the sQGP. The qualitative analysis of the relative importance of different processes in section IV should be understood as an illustration to the above results rather than a quantitative prediction for the dilepton yield from heavy-ion collisions.

Section V is devoted to analyzing the effect of finite quark and gluon widths on the dilepton rate. In Section VI we summarize the main results and their possible applications.

II. DILEPTONS FROM PERTURBATIVE PARTONS

In the present Section, we consider the following partonic mechanisms for dilepton production in pQCD:

1. the Drell-Yan mechanism of quark annihilation ($q + \bar{q} \rightarrow \gamma^*$),
2. quark + anti-quark annihilation with gluon Bremsstrahlung in the final state ($q + \bar{q} \rightarrow g + \gamma^*$),
3. Gluon Compton scattering ($q + g \rightarrow \gamma^* + q$ and $\bar{q} + g \rightarrow \gamma^* + \bar{q}$).

A. Drell-Yan mechanism

The leading order pQCD mechanism for the dilepton production in the partonic phase is the same as for the well known Drell-Yan (DY) process [63]: quark and antiquark annihilate into a lepton pair ($q\bar{q} \rightarrow l^+l^-$), as presented by the diagram (a) in Fig 1. The leading order leading twist (LT) pQCD result for the cross section of DY dilepton production is

$$\left(\frac{d^3\hat{\sigma}(q\bar{q} \rightarrow l^+l^-)}{dQ^2 dx_F dq_T^2} \right)_{\text{on-shell}}^{\text{DY}} = \frac{4\pi\alpha^2 e_q^2}{9Q^4} \frac{x_1 x_2}{x_1 + x_2} (1 - x_1 x_2) \times \delta(q_T^2) \delta(Q^2 - x_1 x_2 S_{NN}) \delta\left(x_F - \frac{x_2 - x_1}{1 - x_1 x_2}\right) \quad (1)$$

where α is the electromagnetic fine structure constant, e_q the fractional quark charge, the subscript ‘on-shell’ stands for ‘leading twist’, the lepton pair has invariant mass Q^2 and transverse momentum q_T .

In collinear pQCD, the off-shellness, mass and transverse momentum of the annihilating quark and antiquark are neglected, and, therefore, the incoming parton momenta are related to the momenta of colliding nuclei as $p_{q(\bar{q})} = x_i P_A/A$. In this case, the parton momentum fractions x_1 and x_2 are related to the virtuality and x_F of the produced photon as (cf. delta-functions in (1)):

$$Q^2 = s = x_1 x_2 S_{NN}; \quad (2)$$

$$x_F = (x_2 - x_1)/(1 - x_1 x_2). \quad (3)$$

Note that the denominator of the x_F definition in (3) is omitted in some works, where an approximate definition $x_F \approx 2p_z/\sqrt{S_{NN}}$ is used instead of $x_F = q_z/(q_z)_{max}$, s denotes the invariant energy for the partonic process, S_{NN} – for the hadronic one. The kinematical limits for this process are

$$S_{NN} \geq Q^2, \quad |x_F| \leq 1, \quad s = Q^2. \quad (4)$$

B. Gluon Bremsstrahlung

The cross section of the *gluon Bremsstrahlung* process $\bar{q}q \rightarrow g + \mu^+ \mu^-$ is [64, 65]

$$\left(\frac{d^2 \hat{\sigma}(q\bar{q} \rightarrow gl^+l^-)}{dQ^2 d \cos \Theta} \right)_{\text{on-shell}}^{\text{gBr}} = \frac{8\alpha^2 e_q^2 \alpha_S}{27Q^2} \frac{s - Q^2}{s^2 \sin^2 \Theta} \times \left(1 + \cos^2 \Theta + 4 \frac{Q^2 s}{(\hat{s} - Q^2)^2} \right), \quad (5)$$

where s is the total energy squared of the colliding partons, and Θ is the scattering angle of the outgoing lepton pair with respect to the incoming quark momentum in the quark center-of-mass system (CMS). Note that the cross section (5) can be written in terms of the Mandelstam variables s , t and u as [20]

$$\begin{aligned} \left(\frac{d^2 \hat{\sigma}(q\bar{q} \rightarrow gl^+l^-)}{dQ^2 dt} \right)_{\text{on-shell}}^{\text{gBr}} &= \frac{8\alpha^2 e_q^2 \alpha_S}{27Q^2} \frac{(t - Q^2)^2 + (u - Q^2)^2}{s^2 tu} \\ &\times \delta(s + t + u - Q^2) \quad (6) \\ &= \frac{8\alpha^2 e_q^2 \alpha_S}{27Q^2 s^2} \left(\frac{t}{u} + \frac{u}{t} + \frac{2sQ^2}{tu} \right) \\ &\times \delta(s + t + u - Q^2), \quad (7) \end{aligned}$$

which coincides with the QED cross section for the virtual Compton scattering up to the color factor and the crossing transformation [66]. Here we denote the momenta of the incoming quark and antiquark as p_1 and p_2 , the momenta of the outgoing gluon as virtual photon as k and q , $s = (p_1 + p_2)^2$, $t = (p_1 - q)^2$, $u = (p_2 - q)^2$. The δ -function $\delta(s + u + t - Q^2)$ reflects the on-shell condition for the partons:

$$p_1^2 + p_2^2 + k^2 = 0. \quad (8)$$

The collinear divergence of the gluon Bremsstrahlung cross section for $t \rightarrow 0$ and $u \rightarrow 0$ (i.e. $\cos \Theta \rightarrow \pm 1$) is obvious; a cut-off Λ^2 on t can be used in order to regularize it:

$$t \leq -\Lambda^2, \quad (9)$$

$$t \geq -s + Q^2 + \Lambda^2. \quad (10)$$

Since in the CMS of the colliding partons we have

$$t = Q^2 - \sqrt{s}q^0 + \sqrt{s}|\vec{q}|\cos \Theta, \quad (11)$$

the corresponding cut-off with respect to $\cos \Theta$ is

$$|\cos \Theta| \leq \frac{(\sqrt{s}q^0 - Q^2 - \Lambda^2)}{\sqrt{s}|\vec{q}|}. \quad (12)$$

Another divergence in the perturbative expression (6) is the infrared (IR) divergence for the energy of the gluon $k^0 \rightarrow 0$ due to the vanishing quark and gluon masses. Indeed, if all the partonic masses (virtualities) are neglected, we have in the CMS:

$$t = k^0(-\sqrt{s} + \sqrt{s}\cos \Theta_2) \rightarrow 0 \text{ at } k^0 \rightarrow 0. \quad (13)$$

This divergence can be remedied by introducing a small finite gluon mass μ_{cut} (cf. the plasmon mass in [22]). Indeed, the gluon thermal mass μ plays the role of a natural cut-off in the sQGP (cf. section III B).

C. Gluon Compton scattering

In QED, the Compton process refers to elastic scattering of a photon off a charged object, and has proven to be very important as it provided early evidence that the electromagnetic wave is quantized [67, 68]. In QCD, the corresponding process is the *gluon Compton scattering* $g + q(\bar{q}) \rightarrow q(\bar{q}) + \gamma^*$. The cross section in leading twist of pQCD [64] is given by:

$$\begin{aligned} \left(\frac{d^2 \hat{\sigma}(g + q)}{dQ^2 d \cos \Theta} \right)_{\text{on-shell}}^{\text{GCS}} &= \frac{\alpha^2 e_q^2 \alpha_S}{18Q^2} \frac{s - Q^2}{s^2(1 + \cos \Theta)} \times \\ &\left\{ \frac{2s}{s - Q^2} + \frac{s - Q^2}{2s}(1 + \cos \Theta)^2 \right. \\ &\left. - \frac{2Q^2}{s}(1 - \cos \Theta) \right\}. \quad (14) \end{aligned}$$

In terms of Mandelstam variables [20] it reads:

$$\begin{aligned} \left(\frac{d\hat{\sigma}(g + q)}{dQ^2 dt} \right)_{\text{on-shell}}^{\text{GCS}} &= \frac{e_q^2 \alpha^2 \alpha_S}{9Q^2} \frac{s^2 + t^2 + 2Q^2 u}{-s^3 t} \\ &\times \delta(s + t + u - Q^2), \quad (15) \end{aligned}$$

which is obviously related by crossing transformation to (7).

III. DILEPTONS FROM DYNAMICAL QUASI-PARTICLES

Let us now proceed to the calculation of the dilepton production by effective strongly interacting partonic quasiparticles with broad spectral functions. Dilepton radiation by the dynamical quasiparticles proceeds via the elementary processes illustrated in Figs. 1 and 2: the basic Drell-Yan $q + \bar{q}$ annihilation mechanism, Gluon Compton scattering ($q + g \rightarrow \gamma^* + q$ and $\bar{q} + g \rightarrow \gamma^* + \bar{q}$), quark + anti-quark annihilation with gluon bremsstrahlung in the final state ($q + \bar{q} \rightarrow g + \gamma^*$) and gluon decay ($g \rightarrow q + \bar{q} + l^+ + l^-$).

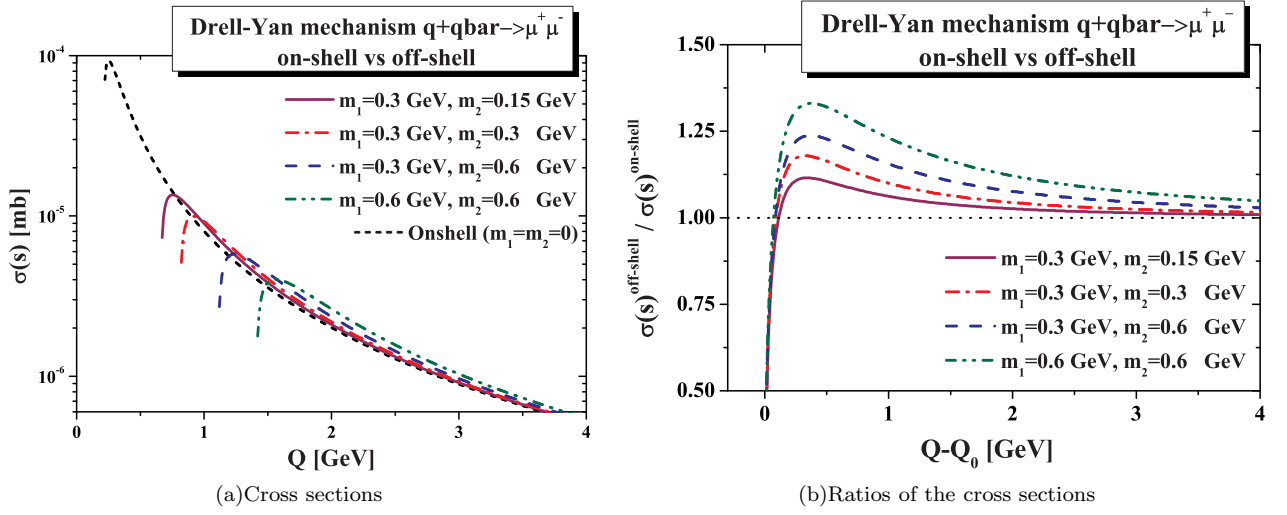


FIG. 3: (color online) Dimuon production cross sections in the Drell-Yan channel ($q+\bar{q}\rightarrow\mu^++\mu^-$). **L.h.s.** The cross section is presented versus the mass of the muon pair Q . The short dashes (black) line shows the on-shell, i.e. the standard perturbative result. The other lines show the off-shell cross section, in which the annihilating quark and antiquark have finite masses m_1 and m_2 with different values: $m_1 = 0.3$ GeV, $m_2 = 0.15$ GeV (solid magenta line), $m_1 = 0.3$ GeV, $m_2 = 0.3$ GeV (dash-dotted red line), $m_1 = 0.3$ GeV, $m_2 = 0.6$ GeV (dashed blue line), $m_1 = 0.6$ GeV, $m_2 = 0.6$ GeV (dash-dot-dot green line). **R.h.s.** The ratio of the off-shell cross section to the on-shell result for the different values of quark and antiquark masses is plotted versus $Q - Q_0$, where Q_0 is the threshold value for the lepton pair mass. Line coding as in the figure on the l.h.s.

A. Off-shell $q + \bar{q}$ in the Drell-Yan mechanism

For the diagram (a) in Fig. 1 the off-shell cross section was obtained in [53] as:

$$\left(\frac{d^3\hat{\sigma}(m_1, m_2, \vec{p}_1, \vec{p}_2)}{dQ^2 dx_F dq_T^2}\right)_{off-shell}^{DY} = \kappa' \left[2Q^4 - Q^2(m_1^2 - 6m_1m_2 + m_2^2) - (m_1^2 - m_2^2)^2 \right] \times \delta(Q^2 - m_1^2 - m_2^2 - 2(p_1 \cdot p_2)) \times \delta\left(x_F - \frac{\sqrt{s}}{s - Q^2}(p_{2z} - p_{1z})\right) \times \delta\left(q_T^2 - (\vec{p}_{1\perp} + \vec{p}_{2\perp})^2\right), \quad (16)$$

with

$$\kappa' = \frac{2\pi\alpha^2 e_q^2}{3Q^4 N_c 8\sqrt{(p_1 \cdot p_2)^2 - m_1^2 m_2^2}}. \quad (17)$$

In (16), N_c is the number of colors, $e_q(-e_q)$ is the fractional charge of the quark (antiquark), m_i^2 are the virtualities of the annihilating quark and antiquark, p_i are their 4-momenta.

Just as in the standard pQCD ‘on-shell’ case, the mass of the produced dilepton pair is fixed to the invariant energy of the quark-antiquark collision:

$$s = Q^2. \quad (18)$$

However, the kinematical limit for the minimal dilepton mass is now higher than in the on-shell case:

$$Q_0^2 \equiv s_0 = (m_1 + m_2 + 2m_{lept})^2 > 4m_{lept}^2, \quad (19)$$

where m_{lept} is the mass of an electron or muon. Also, the incident current also changes in the off-shell case:

$$J = \frac{1}{2}\sqrt{(k_1 \cdot k_2)^2 - m_1^2 m_2^2} = \frac{1}{2}\sqrt{(s - m_1^2 - m_2^2)^2 - 4m_1^2 m_2^2},$$

compared to $J = s/2$ in the on-shell approximation.

The approximation $m_1 = m_2 \rightarrow 0$ in formula (16) is equivalent to restricting oneself to the leading term in the twist expansion, that is, in the case of the unpolarized Drell-Yan process, an expansion in powers of $1/Q$. One can see that in this limit and additionally using the collinear kinematics $\vec{p}_{1\perp} = \vec{p}_{2\perp} = 0$ we recover the standard pQCD result (1).

The off-shell cross sections are compared to the leading twist results in Fig. 3. Dimuon production cross sections in the Drell-Yan mechanism is plotted on the l.h.s. of Fig. 3 versus the mass of the muon pair $Q = \sqrt{s}$. The short dashes (black) line shows the on-shell, i.e. the standard perturbative result. The other lines show the off-shell cross section, in which the annihilating quark and antiquark have finite masses m_1 and m_2 with different values: $m_1 = 0.3$ GeV, $m_2 = 0.15$ GeV (solid magenta line), $m_1 = 0.3$ GeV, $m_2 = 0.3$ GeV (dash-dotted red line), $m_1 = 0.3$ GeV, $m_2 = 0.6$ GeV (dashed blue line), $m_1 = 0.6$ GeV, $m_2 = 0.6$ GeV (dash-dot-dot green line).

The importance of higher twist corrections in the Drell-Yan process is illustrated by the ratio of the off-shell and on-shell integrated cross section $\sigma(Q)$ on the r.h.s. of Fig. 3. The ratio of the off-shell cross section to the on-shell result for the different values of quark and antiquark masses is plotted versus $Q - Q_0$, where Q_0 is the threshold value for the lepton pair mass. Line coding as in the

figure on the previous figure. With increasing Q^2 , off-shell cross sections approach the leading twist – on-shell – result.

In Ref. [60], a model for implementing the higher twist corrections to the Drell-Yan process $p + \bar{p} \rightarrow l^+ + l^- + X$ was formulated making use of the above cross section, a Breit-Wigner parametrization for the quark spectral function and non-integrated parton distributions. The effect of quark off-shellness on the transverse momentum spectrum of the dileptons produced in $p\bar{p}$ collisions was found to be large at low q_T and Q^2 . The calculations were compared to the data on the triple differential Drell-Yan cross section $d^3\sigma/dQ^2 dx_F dq_T$ from experiment E866 [69] at Fermilab in pp collisions at 800 GeV incident energy. Both the slope and magnitude of the q_T distribution of the Drell-Yan pairs were described by the adjustment of the spectral function parametrization. The distribution of the transverse momentum of lepton pairs produced in the Drell-Yan process off *nuclei* $pA \rightarrow l^+l^-X$ was also reproduced within this model [53]. However, the effect of quark off-shellness on the dilepton emission in *heavy-ion collisions* ($A + A$) has not been studied until now. This question can be addressed by convoluting the off-shell cross section (16) with effective spectral functions $A(m_i)$ for quarks in plasma and with a model for the distribution of quarks in plasma (cf. Sections IV and V).

B. Off-shell gluon Bremsstrahlung $q\bar{q} \rightarrow gl^+l^-$

In contrast to the off-shell cross section for the $q\bar{q} \rightarrow l^+l^-$ process, the off-shell cross section for the $q\bar{q}$ annihilation *with gluon Bremsstrahlung* in the final state has not been calculated elsewhere. Therefore, we will provide here a short description of its evaluation.

Starting from the formula for the unpolarized cross section

$$d\sigma = \frac{\sum |\bar{M}_{i \rightarrow f}^-|^2 \varepsilon_1 \varepsilon_2 \Pi \frac{d^3 p_f}{(2\pi)^3}}{\sqrt{(p_1 p_2)^2 - m_1^2 m_2^2}} (2\pi)^4 \delta(p_1 + p_2 - \Sigma p_f), \quad (20)$$

where the incoming quark and antiquark momenta are p_1 and p_2 , their masses m_1 and m_2 , respectively; p_f are

the momenta of the outgoing particles, i.e. of the electron (muon) and positron (anti-muon) and gluon, we note that the dilepton production cross section can be easily obtained from the cross section for the production of virtual photons as

$$\frac{d\sigma(l^+l^-)}{dQ^2 dt} = \frac{\alpha}{3\pi Q^2} \frac{d\sigma(\gamma^*)}{dt} FF(Q^2, Q_0^2) \quad (21)$$

with

$$FF(Q^2, Q_0^2) = \sqrt{1 - \frac{Q_0^2}{Q^2}} \left(1 + \frac{Q_0^2}{2Q^2}\right), \quad (22)$$

where $Q_0^2 = 4m_{lept}^2$, m_{lept} is the lepton mass.

Furthermore, we define the momenta of the internal quark exchanged in the two relevant diagrams (see Fig. 1) as $p_3 \equiv p_1 - q$, $\bar{p}_3 \equiv p_1 - p_2 - p_3$ and its mass as m_3 . The final gluon momentum is k and its mass is μ . Then the matrix element of the process $q + \bar{q} \rightarrow g + \gamma^*$ is

$$M = M_a + M_b, \quad (23)$$

where

$$M_a = -e_q e g_s T_{ij}^l \frac{\epsilon_\nu(q) \epsilon_{\sigma l}(k)}{\hat{p}_3^2 - m_3^2} \times u_i(p_1, m_1) [\gamma^\nu (\hat{p}_3 + m_3) \gamma^\sigma] v_j(p_2, m_2) \quad (24)$$

and

$$M_b = -e_q e g_s T_{ij}^l \frac{\epsilon_{\sigma l}(k) \epsilon_\nu(q)}{\hat{\bar{p}}_3^2 - m_3^2} \times u_i(p_1, m_1) [\gamma^\sigma (\hat{\bar{p}}_3 + m_3) \gamma^\nu] v_j(p_2, m_2), \quad (25)$$

e is the electron charge; e_q is the quark fractional charge; T_{ij}^l is the generator of the SU(3) color group (that will yield the color factor in the cross section); $\epsilon_\nu(q)$ is the polarization vector for the virtual photon with momentum q ; $\epsilon_{\sigma l}(k)$ is the polarization vector for the gluon of momentum k and color l ; $u_i(p, m)$ is a Dirac spinor for the quark with momentum p , mass m and color i ; and $v_i(p, m)$ is the spinor for the anti-quark.

The squared – and summed over spin polarizations as well as over color degrees of freedom – matrix element can be decomposed in the following summands:

$$\sum |M|^2 = \sum M_a^* M_a + \sum M_b^* M_b + \sum M_a^* M_b + \sum M_b^* M_a, \quad (26)$$

where the star denotes the complex conjugation.

The spinors for quark states with mass m_i contribute to the expression for the average matrix element only in the combinations $\sum \bar{u}(p, m_i) u(p, m_i) = (\hat{p} + m_i)$ (cf. [70]) and the correlation functions between the states with different

masses does not enter $|M|^2$. Thus we find:

$$\begin{aligned} \sum M_a^* M_b &= -\frac{e_q^2 e^2 g_s^2 \text{Tr}\{T^2\}}{(p_3^2 - m_3^2)(\bar{p}_3^2 - m_3^2)} \left[\text{Tr} \left\{ (\hat{p}_2 - m_2) \gamma_\sigma (\hat{p}_3 + m_3) \gamma_\nu (\hat{p}_1 + m_1) \gamma^\sigma (\hat{p}_3 + m_3) \gamma^\nu \right\} \right. \\ &\quad - \frac{1}{Q^2} \text{Tr} \left\{ (\hat{p}_2 - m_2) \gamma_\sigma (\hat{p}_3 + m_3) \hat{q} (\hat{p}_1 + m_1) \gamma^\sigma (\hat{p}_3 + m_3) \hat{q} \right\} \\ &\quad - \frac{A}{k^2} \text{Tr} \left\{ (\hat{p}_2 - m_2) \hat{k} (\hat{p}_3 + m_3) \gamma_\nu (\hat{p}_1 + m_1) \hat{k} (\hat{p}_3 + m_3) \gamma^\nu \right\} \\ &\quad \left. + \frac{A}{k^2 Q^2} \text{Tr} \left\{ (\hat{p}_2 - m_2) \hat{k} (\hat{p}_3 + m_3) \hat{q} (\hat{p}_1 + m_1) \hat{k} (\hat{p}_3 + m_3) \hat{q} \right\} \right]. \quad (27) \end{aligned}$$

$$\begin{aligned} \sum |M_a|^2 &= -\frac{e_q^2 e^2 g_s^2 \text{Tr}\{T^2\}}{(p_3^2 - m_3^2)^2} \left[\text{Tr} \left\{ \gamma_\sigma (\hat{p}_3 + m_3) \gamma_\nu (\hat{p}_1 + m_1) \gamma^\nu (\hat{p}_3 + m_3) \gamma^\sigma (\hat{p}_2 - m_2) \right\} \right. \\ &\quad - \frac{1}{Q^2} \text{Tr} \left\{ \gamma_\sigma (\hat{p}_3 + m_3) \hat{q} (\hat{p}_1 + m_1) \hat{q} (\hat{p}_3 + m_3) \gamma^\sigma (\hat{p}_2 - m_2) \right\} \\ &\quad - \frac{A}{k^2} \text{Tr} \left\{ \hat{k} (\hat{p}_3 + m_3) \gamma_\nu (\hat{p}_1 + m_1) \gamma^\nu (\hat{p}_3 + m_3) \hat{k} (\hat{p}_2 - m_2) \right\} \\ &\quad \left. + \frac{A}{k^2 Q^2} \text{Tr} \left\{ \hat{k} (\hat{p}_3 + m_3) \hat{q} (\hat{p}_1 + m_1) \hat{q} (\hat{p}_3 + m_3) \hat{k} (\hat{p}_2 - m_2) \right\} \right]. \quad (28) \end{aligned}$$

Note that by the transformation $\{p_3 \rightarrow \bar{p}_3, p_1 \rightarrow p_2, p_2 \rightarrow p_1, m_1 \rightarrow -m_2, m_2 \rightarrow -m_1\}$ we readily obtain $\sum M_b^* M_a$ from $\sum M_a^* M_b$ and $\sum |M_b|^2$ from $\sum |M_a|^2$. In equations (27) and (28), A sets the gauge. We used the feynpar.m [71] package of the Mathematica program [72] to evaluate the traces of the products of the gamma matrices. The resulting cross section is (here shown at $A = 1$):

$$\begin{aligned} \left(\frac{d\hat{\sigma}(q\bar{q} \rightarrow gl^+l^-)}{dQ^2 dt} \right)_{\text{offshell}}^{gBr} &= -\frac{\alpha^2 \alpha_S e_q^2 \Theta \left(-Q^2 + s + t - \mu^2 \right) \delta(s + t + u - m_1^2 - m_2^2 - Q^2 - \mu^2)}{27 Q^4 \sqrt{-2(m_1^2 m_2^2) + (m_1^2 + m_2^2 - s)^2} s (m_3^2 - t) (m_3^2 - u) \mu^2} \\ &\times \left[m_3^6 \left(s t (s + t) + (s + 2t)^2 u + (s + 4t) u^2 - Q^4 (t + u) + Q^2 (t^2 + u^2) \right) \right. \\ &\quad + t u (-2Q^6 (t + u) + 2t u (2s (s + t) + (2s + t) u) + 4Q^4 (t^2 + u^2 + s (t + u)) \\ &\quad - Q^2 (2s^2 (t + u) + 4s (t^2 + u^2) + (t + u) (2t^2 - 3t u + 2u^2))) + m_3^2 \left(2Q^6 (t + u)^2 \right. \\ &\quad - Q^4 (t + u) (4t (s + t) + (4s + t) u + 4u^2) + 2Q^2 \left(t^4 + t^3 u - t^2 u^2 + t u^3 + u^4 + s^2 (t + u)^2 \right. \\ &\quad \left. \left. + 2s (t + u) (t^2 + u^2) \right) + t u (-3s^2 (t + u) - 2s (t^2 + 3t u + u^2) + 2(t^3 + u^3)) \right) - m_3^4 \left(- \left(s^2 (t - u)^2 \right) \right. \\ &\quad \left. + 2Q^6 (t + u) - 2s (t + u) (t^2 - 3t u + u^2) + t u (3t^2 + 8t u + 3u^2) - Q^4 (5t^2 + 2t u + 5u^2 + 4s (t + u)) \right. \\ &\quad \left. + Q^2 (2s^2 (t + u) + 4s (t^2 + u^2) + 3(t^3 + u^3)) \right) - m_1 m_3 (t u (2Q^4 (t + u) + s^2 (t + u) \\ &\quad - Q^2 (t^2 + 12t u + u^2 + 3s (t + u))) + m_3^2 (t + u) (-2Q^4 (t + u) - s^2 (t + u) + Q^2 (t^2 + 12t u + u^2 \\ &\quad + 3s (t + u))) + m_3^4 (2Q^4 (t + u) + s^2 (t + u) - Q^2 (3s (t + u) + 7(t^2 + u^2)))) \\ &\quad + (- (m_3^6 (6Q^4 + 2s^2 + t^2 + u^2 - 5Q^2 (t + u) + 4s (t + u))) \\ &\quad + t u (-8Q^6 + t u (2s + t + u) + Q^4 (-4s + 7(t + u)) + Q^2 (4s^2 + 2(t - u)^2 + 5s (t + u)))) \\ &\quad + m_3^4 \left(-8Q^6 + 2t(s + t)^2 + (2s^2 + 10st + t^2) u + (4s + t) u^2 + 2u^3 + Q^4 (-4s + 13(t + u)) \right. \\ &\quad \left. + Q^2 (4s^2 + 5s (t + u) - 2(t^2 + 8t u + u^2)) \right) + m_3^2 (8Q^6 (t + u) + Q^4 (-7t^2 - 20t u - 7u^2 + 4s (t + u)) \\ &\quad - t u (2s^2 + 6s (t + u) + 3(t^2 + u^2)) - Q^2 (4s^2 (t + u) + (t + u) (4t^2 - 13t u + 4u^2) + s (7t^2 + 6t u + 7u^2))) \\ &\quad + m_1 m_3 \left(- (m_3^4 (10Q^4 - 2s^2 + t^2 + u^2 - s (t + u) + 2Q^2 (2s + t + u))) - t u (10Q^4 - 2s^2 + t^2 + u^2 \right. \\ &\quad \left. - s (t + u) + 2Q^2 (2s + t + u)) + m_3^2 (10Q^4 (t + u) + (t + u) (-2s^2 + t^2 + u^2 - s (t + u)) \right) \end{aligned}$$

$$\begin{aligned}
& +4Q^2(-t^2+4tu-u^2+s(t+u)))\mu^2+(m_3^2-t)(m_3^2-u)(4m_1m_3Q^2-12m_3^2Q^2-10Q^4 \\
& -4m_1m_3s+4m_3^2s-6Q^2s+4m_3^2t+3Q^2t-st-t^2+4m_3^2u+3Q^2u-su-4tu-u^2)\mu^4 \\
& +(m_3^2-t)(m_3^2-u)(2(m_1-m_3)m_3-2Q^2+t+u)\mu^6+2m_2^6(m_3^2-t)(m_3^2-u)(2Q^2-s+\mu^2) \\
& +m_2^4(m_3^2-t)(m_3^2-u)(2m_1m_3Q^2+2m_3^2Q^2+4Q^4-6Q^2s+2s^2-5Q^2t+2st-5Q^2u+2su \\
& -2(m_3(m_1+m_3)+t+u)\mu^2-4\mu^4)-2m_2^5(m_3^2-t)(m_3^2-u)(m_1s+m_3(3Q^2-2s+3\mu^2)) \\
& -2m_2^3(m_3^2-t)(m_3^2-u)(-(m_1s(-Q^2+s+t+u-\mu^2))+m_3(Q^4 \\
& -3Q^2(s+t+u)+2s(s+t+u)-3(s+t+u)\mu^2+\mu^4))-m_2^2(m_3^2-t)(m_3^2-u)(2stu+(4s^2 \\
& -2tu+3s(t+u))\mu^2-5(2s+t+u)\mu^4+6\mu^6+5Q^4(t+u-2\mu^2)-2m_3^2(Q-\mu)(Q+\mu)(2Q^2 \\
& -2s-t-u+2\mu^2)-Q^2(5t^2-2tu+5u^2+5s(t+u)+2s\mu^2-8(t+u)\mu^2+2\mu^4)+2m_1m_3(s^2 \\
& -(3s+t+u)\mu^2+2\mu^4+Q^2(-s+t+u-4\mu^2))) -m_2(m_1(-2m_3^6(Q^4-2Q^2(s-5\mu^2)+(s-\mu^2)^2) \\
& +tu(2stu+(t-u)^2+s(t+u))\mu^2-(t+u)\mu^4-Q^4(t+u-4\mu^2)+Q^2((t-u)^2+s(t+u) \\
& -26(t+u)\mu^2+4\mu^4))+m_3^4(2stu+2s^2(t+u)+(t-u)^2\mu^2-3s(t+u)\mu^2+(t+u)\mu^4 \\
& +Q^4(t+u+4\mu^2)+Q^2((t-u)^2-3s(t+u)-6(t+u)\mu^2+4\mu^4)))+m_3^2(-2stu(s+t+u) \\
& -(t-u)^2(s+t+u)\mu^2+(t^2+u^2)\mu^4+Q^4(t^2+u^2-4(t+u)\mu^2)+Q^2(-((t-u)^2(s+t+u)) \\
& -2(5t^2-52tu+5u^2)\mu^2-4(t+u)\mu^4))) +m_3(tu(-4Q^6-4stu+Q^4(8s+t+u)+Q^2(-4s^2+t^2 \\
& +4tu+u^2-s(t+u))) - (12t^2(s+t)^2+t(-4Q^4+4s^2+19st+17t^2+Q^2(-12s+8t))u+(12s^2 \\
& +8Q^2t+19st-4t^2)u^2+(24s+17t)u^3+12u^4)\mu^2+tu(4Q^2+8s+t+u)\mu^4-4tu\mu^6 \\
& +m_3^2(-((t+u)(-4Q^6-4stu+Q^4(8s+t+u)+Q^2(-4s^2+t^2+4tu+u^2-s(t+u)))) \\
& +(-4Q^4(t+u)+28s^2(t+u)+(t+u)(23t^2+8tu+23u^2)+s(49t^2+74tu+49u^2) \\
& +4Q^2(t+u)(-3s+2(t+u)))\mu^2-(t+u)(4Q^2+8s+t+u)\mu^4+4(t+u)\mu^6)+m_3^4(-4Q^6 \\
& -4stu-(28s^2+11t^2+32tu+11u^2+43s(t+u))\mu^2+(8s+t+u)\mu^4-4\mu^6+Q^4(8s+t+u+4\mu^2) \\
& +Q^2(-4s^2+t^2+4tu+u^2-8(t+u)\mu^2+4\mu^4-s(t+u-12\mu^2)))))] \quad (29)
\end{aligned}$$

In the off-shell case, the dilepton mass range is $4m_{lept}^2 < Q^2 < (\sqrt{s} - m_q)^2$, while the kinematical limits for the momentum transfer t are

$$t_{min}^{max} = -\frac{s}{2}(C_1 \pm C_2), \quad (30)$$

where

$$\begin{aligned}
C_1 &= 1 - (\beta_1 + \beta_2 + \beta_3 + \beta_4) + (\beta_1 - \beta_2)(\beta_3 - \beta_4), \\
C_2 &= \sqrt{(1 - \beta_1 - \beta_2)^2 - 4\beta_1\beta_2} \\
& \quad \times \sqrt{(1 - \beta_3 - \beta_4)^2 - 4\beta_3\beta_4} \quad (31)
\end{aligned}$$

with

$$\beta_1 = m_1^2/s, \quad \beta_2 = m_2^2/s, \quad \beta_3 = Q^2/s, \quad \beta_4 = \mu^2/s. \quad (32)$$

Additionally, we note that there is a threshold in the CMS energy \sqrt{s} for the $q + \bar{q}$ interaction:

$$s \geq \max\{(m_1 + m_2)^2, (\mu + Q)^2\}. \quad (33)$$

One can easily check that the expression (29) for $m_i \rightarrow 0$ approaches the leading twist pQCD result, where

$\mu_{cut} = \mu$. We illustrate this in Fig. 4. In Fig. 4, the off-shell cross sections for the quark annihilation with gluon bremsstrahlung mechanism at various values of quark and gluon off-shellnesses (masses) are compared to the on-shell (pQCD) result. Dashed black line shows the on-shell cross section with $\mu_{cut} = 0.206$ GeV, red solid line presents the off-shell cross section for the gluon mass fixed to $\mu = 0.8$ GeV and on-shell quark and anti-quark ($m_1 = m_2 = m_3 = 0$). Blue dash-dotted line gives the off-shell result for $\mu = 0.8$ GeV, $m_1 = m_2 = m_3 = m_q = 0.6$ GeV. One readily notices the shift of the maximum allowed mass of the pair to a lower value (in order to produce a massive gluon in the final state). For the rest of the Q values, the effect of the quark and gluon off-shellness reaches at most 50%, as is seen in the ratios of the cross sections, plotted in the r.h.s. of Fig. 4.

Next we compare the double differential off-shell and on-shell cross sections. The results for the transverse momentum distributions of the dileptons are presented in Fig. 5. Solid black line shows the differential on-shell cross section with $\mu_{cut} = 0.206$ GeV, blue dashed line

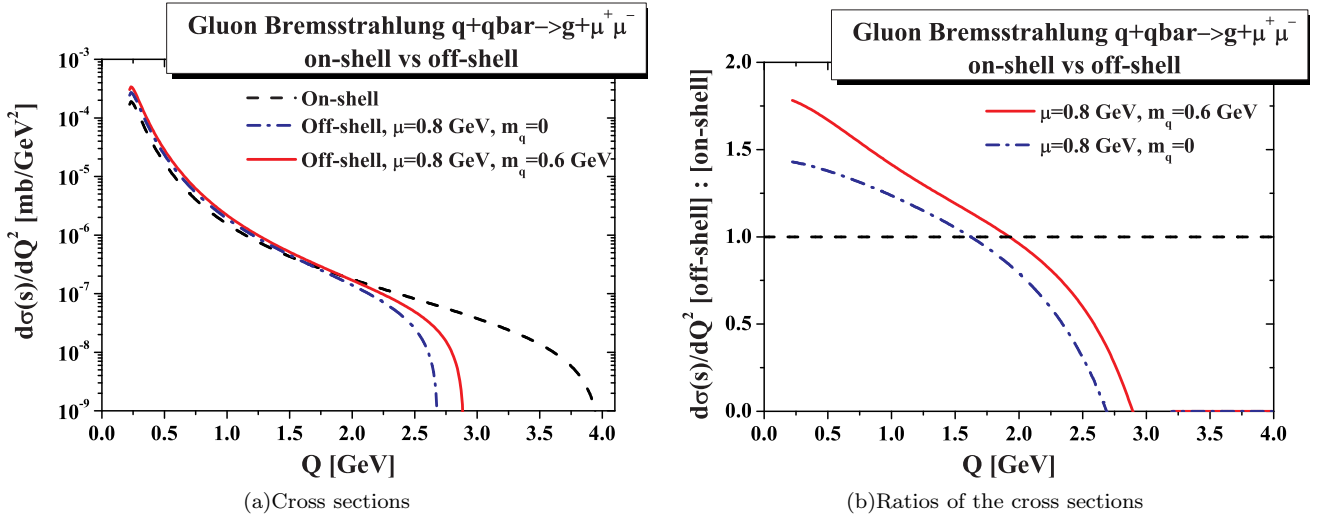


FIG. 4: (color online) Comparison of off-shell and on-shell gluon Bremsstrahlung $q + \bar{q} \rightarrow g + \mu^+ \mu^-$ cross sections at $\sqrt{s} = 4$ GeV. **L.h.s.** Dashed black line shows the on-shell cross section with $\mu_{cut} = 0.206$ GeV, blue dash-dotted line presents the off-shell cross section for the gluon mass fixed to $\mu = 0.8$ GeV and on-shell quark and anti-quark ($m_1 = m_2 = m_3 = 0$). Red solid line gives the off-shell result for $\mu = 0.8$ GeV, $m_1 = m_2 = m_3 = m_q = 0.6$ GeV. **R.h.s.** The ratio of off-shell to on-shell cross sections. Line coding is as on the l.h.s. plot.

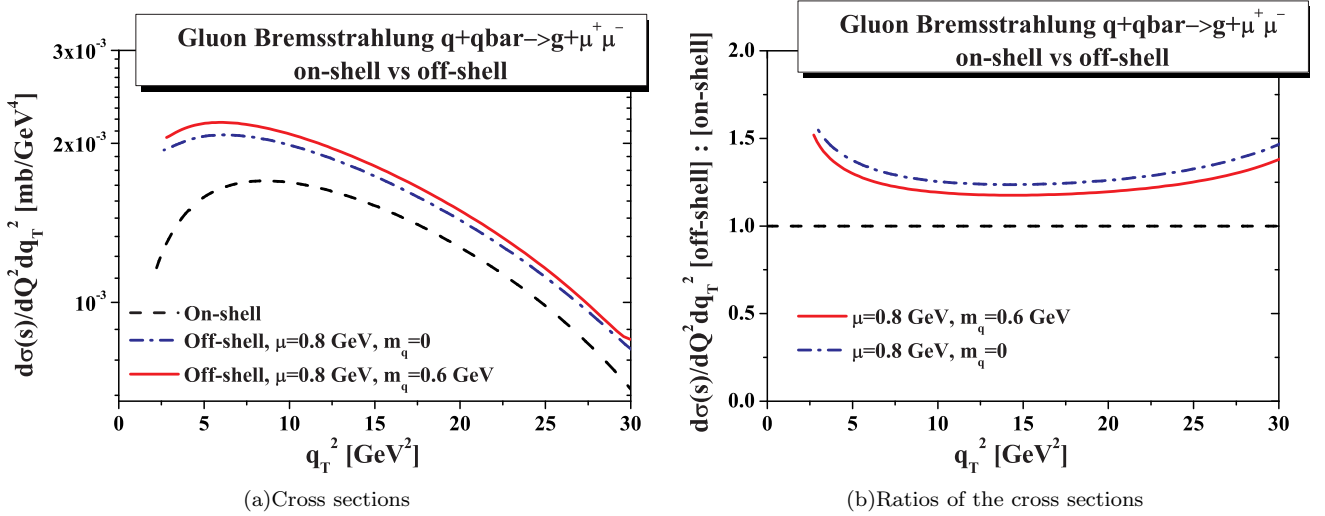


FIG. 5: (color online) Comparison of the transverse momentum distributions of muon pairs produced in the gluon Bremsstrahlung $q + \bar{q} \rightarrow g + \mu^+ \mu^-$ channel in the off-shell and on-shell cases. **L.h.s.** Dashed black line shows the differential on-shell cross section with $\mu_{cut} = 0.206$ GeV, blue dash-dotted line presents the off-shell cross section for the gluon mass fixed to $\mu = 0.8$ GeV and on-shell quark and anti-quark ($m_1 = m_2 = m_3 = 0$). Red solid line gives the off-shell result for $\mu = 0.8$ GeV, $m_1 = m_2 = m_3 = m_q = 0.6$ GeV. **R.h.s.** The ratio of off-shell to on-shell cross sections. Line coding is as on the l.h.s. plot.

presents the off-shell cross section for the gluon mass fixed to $\mu = 0.8$ GeV and on-shell quark and anti-quark ($m_1 = m_2 = m_3 = 0$). Red dash-dotted line gives the off-shell result for $\mu = 0.8$ GeV, $m_1 = m_2 = m_3 = m_q = 0.6$ GeV. Again, we find the largest effect on the edge of the phase space, at the minimal q_T .

C. Off-shell gluon Compton scattering $gq \rightarrow ql^+l^-$

The cross section for the gluon Compton scattering can be calculated analogously to the calculation of the gluon Bremsstrahlung cross section (29) above. On the other hand, the cross sections for $g + q \rightarrow q + l^+ + l^-$ and $g + \bar{q} \rightarrow \bar{q} + l^+ + l^-$ is readily obtained from (29) by the crossing transformation.

Kinematic limits on s , t , Q^2 in the off-shell GCS pro-

cess are analogous to the $q + \bar{q}$ case. In the off-shell case, the dilepton mass range is $4m_{lept}^2 < Q^2 < (\sqrt{s} - m_q)^2$, while the kinematical limits on the momentum transfer t are given by the formulae (30)-(31) with

$$\beta_1 = m_1^2/s, \beta_2 = \mu^2/s, \beta_3 = Q^2/s, \beta_4 = m_2^2/s, \quad (34)$$

while

$$s \geq \max\{(m_1 + \mu)^2, (m_2 + Q)^2\}.$$

D. Virtual gluon decay $g \rightarrow q\bar{q}l^+l^-$ and virtual quark decay $q \rightarrow gq l^+l^-$

Although the process of real gluon decay $g \rightarrow q + \bar{q} + l^+l^-$ is forbidden kinematically for perturbative particles, it has a finite region of validity, if the gluon is off-shell, due to its broad width and finite pole mass. Analogously, the virtual quark decay is also possible in the off-shell case. We present the Feynman diagrams for the corresponding processes in Fig. 2. The off-shell cross section for these processes can straightforwardly be obtained from (29) by the crossing relation. For example, the cross section for $q \rightarrow gq l^+l^-$ is obtained from $q \rightarrow gl^+l^-$ by changing $p_2 \rightarrow -p_2$.

Note that, in order to obtain the dilepton rates, the elementary cross sections have to be consequently convoluted with the effective spectral functions for quarks and gluons. The magnitude and shape of the contributions of the virtual decays to the dilepton rates is very sensitive to the final choice of the spectral function. In the DQPM the contribution from gluon decay is higher than that from virtual quark decay, since the gluonic quasi-particles are more massive and broader than the quarks [43], and thus the kinematically allowed region is larger for the virtual gluon than for the virtual quark decay.

On the other hand, within the DQPM parametrizations for the partonic spectral functions, both processes presented by the diagrams in Fig. 2 generate little dilepton yield anywhere except the extremely low masses: $Q \approx 2m_{muon}$. Therefore, we refrain from plotting here the contributions explicitly and also do not consider them in the next section dedicated to the comparison of the yields from different mechanisms.

IV. CONTRIBUTIONS OF THE DIFFERENT PROCESSES TO THE DILEPTON RATES FROM QGP

In the following we are interested in the relative importance of the different processes and their contributions to the dilepton yield of the strongly coupled quark-gluon plasma.

Due to the factorization property proven in [22], the dilepton emission from the QGP created in the heavy-ion

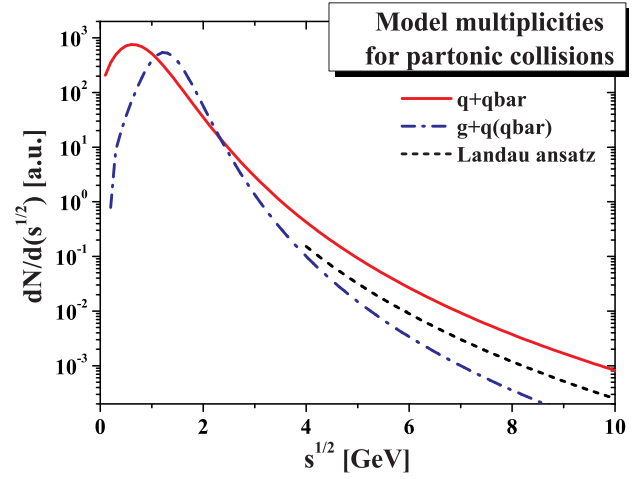


FIG. 6: (color online) Multiplicities of $q + \bar{q}$ and $g + q(g + \bar{q})$ collisions. The red solid line represents the multiplicities of the $q + \bar{q}$ collisions and the blue dashed line represents the probability for the gluon+quark(antiquark) interaction. The black dashed line shows for comparison the prediction in the Landau model for the heavy-ion collision – the power law fall as $(\sqrt{s})^{-7}$.

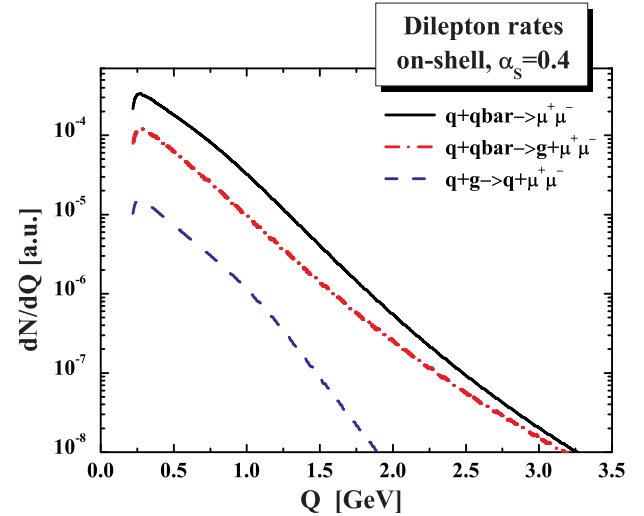


FIG. 7: (color online) Dimuon rates dN/dQ from QGP calculated using the cross sections in the on-shell approximation, $\alpha_S = 0.4$. Black solid line shows the contribution of the Drell-Yan channel ($q + \bar{q} \rightarrow \mu^+ \mu^-$), red dash-dotted line represents the contribution of the channel $q + \bar{q} \rightarrow g + \mu^- \mu^+$, blue dashed line shows the contribution of the channel $q + g \rightarrow q + \mu^+ \mu^-$. The rates are in ‘arbitrary units’, reflecting our use of simplistic quark and gluon distributions in the QGP.

collision is given by the convolution of the elementary sub-process cross sections (describing quark/gluon interactions resulting in the emission of dileptons) with the structure functions that characterize the properties and evolution of the plasma (encoded in the distribution of the quarks and gluons with different momenta and vir-

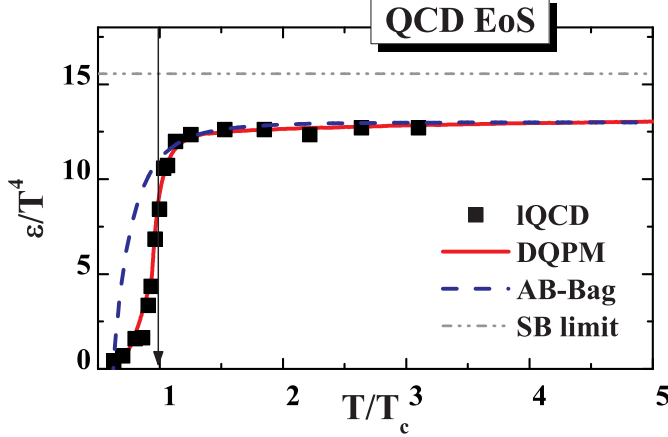


FIG. 8: (color online) QCD energy density versus temperature from lattice QCD (square symbols) [73], the DQPM approach (red solid line) [43] and the ‘AB-Bag’ model (blue dashed line) [74]. The grey dash-dotted line shows the Stefan-Boltzmann limit. The arrow indicates the critical temperature.

tualities):

$$\frac{d^3\sigma_{\text{QGP}}}{dQ^2 dx_F dq_T^2} = \sum_{abc} \int d\hat{s} \int_0^\infty dm_1^i \int_0^\infty dm_2^i \int_0^\infty d\mu^f F_{ab}(\hat{s}, m_1^i, m_2^i) \times A_c(\mu^f) \frac{d^3\hat{\sigma}_{abc}(\hat{s}, m_1^i, m_2^i, \mu^f)}{dQ^2 dx_F dq_T^2}, \quad (35)$$

where m_1^i and m_2^i are the off-shellnesses (i.e. virtualities) of the incoming partons, μ^f in the off-shellness of the outgoing parton, the indices a, b, c denote quark, antiquark or gluon so that all the considered mechanisms are covered. The cross sections $\hat{\sigma}_{abc}(\hat{s}, m_1^i, m_2^i, \mu^f)$ for the different processes have been derived in the previous Section.

In (35), we integrate over the motion of partons, but also over their virtualities by employing phenomenological structure functions F_{ab} that depend on the invariant energy \hat{s} of the partonic sub-process as well as on the virtualities of the incoming partons and the spectral function $A(\mu^f)$ for the virtuality distribution of the parton in the final state. Here should in principle be a two particle correlator, but we work in the 2PI approximation so that the parton in the sQGP can be characterized by a single-particle distribution, therefore we assume that the plasma structure function can be approximated by

$$F_{ab}(\hat{s}, m_1, m_2) = A_a(m_1)A_b(m_2) \frac{dN_{ab}}{ds}. \quad (36)$$

In this context, the quantity $dN_{q\bar{q}}/ds$ has the meaning of the average multiplicity of $q + \bar{q}$ collisions in the plasma

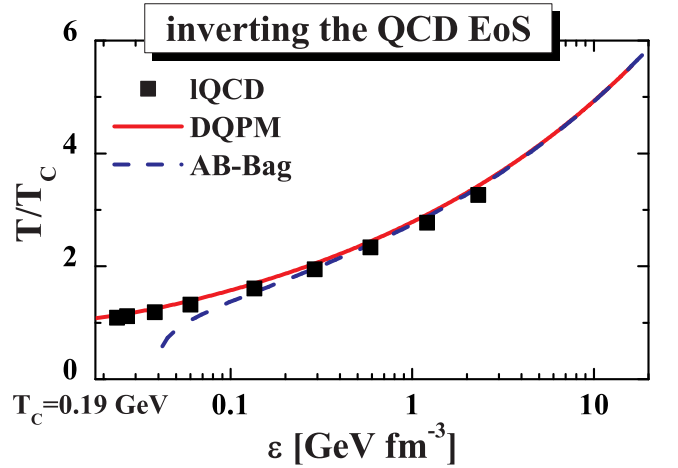


FIG. 9: (color online) Temperature as a function of the energy density from lattice QCD (square symbols) [73], the DQPM approach (red solid line) [43] and the ‘AB-Bag’ model (blue dashed line) [74].

as a function of the invariant energy of these collisions. Analogously, dN_{gq}/ds denotes the multiplicity of $g + q$ collisions.

In order to address the relative importance of the different mechanisms for the dilepton production in the sQGP, we need a quantitative model for the multiplicities of the collisions $q + \bar{q}$ and $g + q$ ($g + \bar{q}$) as functions of the center-of-mass energy \sqrt{s} of these collisions. For this aim, we use the parametrizations, presented in Fig. 6. Inspired by the Landau model for heavy ion collisions, the parametrizations fall off with temperature according to the power law $\phi(T) \sim T^{-7}$ [4], while the magnitude of the distributions depend on the total available energy ($\sim s_{NN}$). Additionally, we notice that the energy of parton collisions is on average proportional to the temperature $\sqrt{s} \sim T$. In this admittedly very simplified picture, the functional form for $dN/d\sqrt{s}$ is taken as

$$\frac{dN}{d\sqrt{s}} = N_0 s^{1/4} [(\sqrt{s} - P)^2 + W]^{-3.5}. \quad (37)$$

By choosing ($P_{q\bar{q}} = 0.5$, $W_{q\bar{q}} = 1.2$) for $q\bar{q}$ collisions and ($P_{gq} = 1.2$, $W_{gq} = 0.6$) for gq collisions, we adjust the maximum of $dN(q + \bar{q})$ to $\sqrt{s} \approx 0.5$ GeV and shift the maximum of $dN(g + q)$ to $\sqrt{s} \approx 1.2$ GeV, reflecting the fact that the threshold $\sqrt{s_0} = m_a + m_b$ is higher for gq than for $q\bar{q}$ collisions. Indeed, the gluonic quasi-particles are expected to be more massive than the quark ones [43]. The parameter N_0 remains to be fixed to experimental data or microscopic calculations, therefore we currently consider the distributions in ‘‘arbitrary units’’. At high \sqrt{s} the distributions approach the Landau ansatz $\text{const} \cdot T^{-7}$, which is shown in Fig. 6 by the black dotted line.

In Fig. 7 we plot the dilepton spectrum, assuming $\alpha_S = 0.4$ [77]. One observes that after the convolution with the distribution of possible \sqrt{s} for the $q + \bar{q}$ annihi-

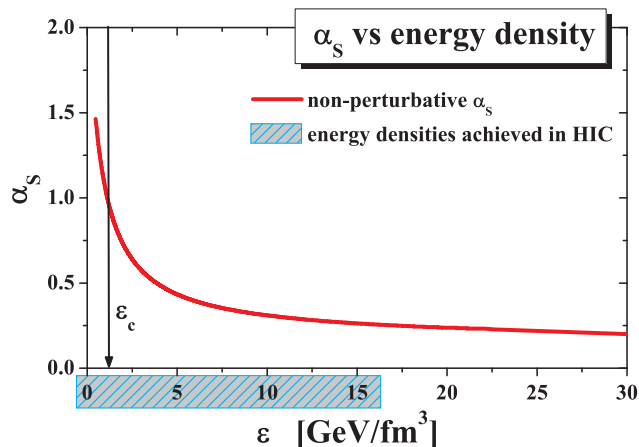


FIG. 10: (color online) Non-perturbative running coupling as a function of the local energy density ε . The shadowed area indicates the energy densities reached in heavy ion collisions at SPS and RHIC. The arrow shows the critical energy-density.

lation in sQGP, the yield of lepton pairs produced in the Bremsstrahlung process is below the leading order DY mechanism contribution. Thus, the DY rate is higher in the magnitude than that of the gluon Bremsstrahlung process despite the fact that the former one contributes only to the lepton pairs with a mass equal to the \sqrt{s} .

On the other hand, one notices from the Fig. 7 that the GCS mechanism is sub-leading, unless the gluonic content of the plasma is orders of magnitude above the quark content, which is achieved neither at SPS nor at RHIC energies. A very high gluon content might be found at LHC, in which case, the GCS process would give a considerable contribution to the dilepton yield of the QGP.

Let us remind that the running coupling α_S depends on the local energy density ε . The DQPM [52] provides a good parametrization of the QCD running coupling as a function of temperature in the non-perturbative regime for temperatures close to T_c (cf. Fig. 1 in Ref. [52]). Note that close to T_c the full coupling calculated on the lattice increases with the decreasing temperature much faster than the pQCD prediction.

The relation between the energy density and temperature, i.e. the equation of state, has also been extracted on the lattice [73] – see Fig. 8. The DQMP model describes the QCD equation of state even at $T \sim T_c$ [43]. A rather simple parametrization for the QCD equation of state – the “AB-Bag model” – is proposed in [74] and provides a good fit of the SU(3) lattice data above T_c ; we extend this model to 3-flavors and also compare to lattice data [73] in Fig 8.

In Fig 9 we reversed the relation and present the temperature as a function of the energy density. Using this relation, we obtain the running coupling as a function of the energy density ε ; we present α_S vs. ε in Fig. 10. On the other hand, simulations in transport theory [75] have shown that the local energy densities achieved in the

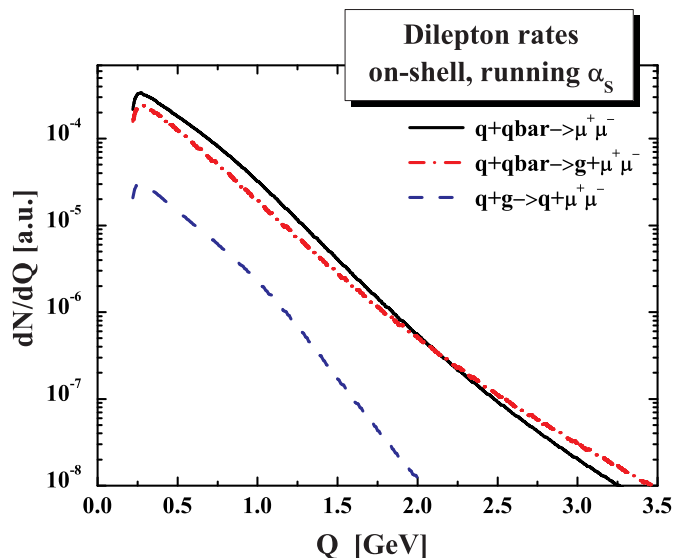


FIG. 11: (color online) Dimuon rates dN/dQ from QGP calculated using the cross sections in the on-shell approximation, $\alpha_S = 0.8$. Black solid line shows the contribution of the Drell-Yan channel ($q + \bar{q} \rightarrow \mu^+ \mu^-$), red dash-dotted line represents the contribution of the channel $q + \bar{q} \rightarrow g + \mu^- \mu^+$, blue dashed line shows the contribution of the channel $q + g \rightarrow q + \mu^+ \mu^-$. The rates are in ‘arbitrary units’, reflecting our use of simplistic quark and gluon distributions in the QGP.

course of heavy-ion collisions at SPS and RHIC energies reach at most 20 GeV/fm^3 ; this region is high-lighted in Fig. 10 by a shadowed area.

One observes that α_S at the energy densities of interest is on average approximately 0.8. Using this value for α_S , we compare the rates in Fig. 11. In this case, the contribution of the $O(\alpha_S)$ diagrams (gluon-Compton scattering $qg \rightarrow q\gamma^*$ and gluon Bremsstrahlung $q\bar{q} \rightarrow g\gamma^*$) is no more subleading to the DY annihilation mechanism!

Next, we plot the dilepton rates – within our approximate model for the parton collision density in the plasma – for the case of massive quarks and gluons in Fig. 12(a). The rates are calculated by convoluting the off-shell cross sections obtained in the previous Section with model $dN/d\sqrt{s}$. Quarks and gluons are massive quasi-particles, quark masses being set to $m_q = 0.3 \text{ GeV}$ and gluon mass $\mu = 0.8 \text{ GeV}$. Black solid line shows the contribution of the Drell-Yan channel ($q + \bar{q} \rightarrow \mu^+ \mu^-$), red dash-dotted line represents the contribution of the channel $q + \bar{q} \rightarrow g + \mu^- \mu^+$, blue dashed line shows the contribution of the channel $q + g \rightarrow q + \mu^+ \mu^-$. The rates in the three channels are modified compared to the massless case (cf. Fig. 11). In particular, we point to the clear threshold behavior of the Born (Drell-Yan) term, noted also by the authors that have studies the dilepton production by massive partons previously [43–45].

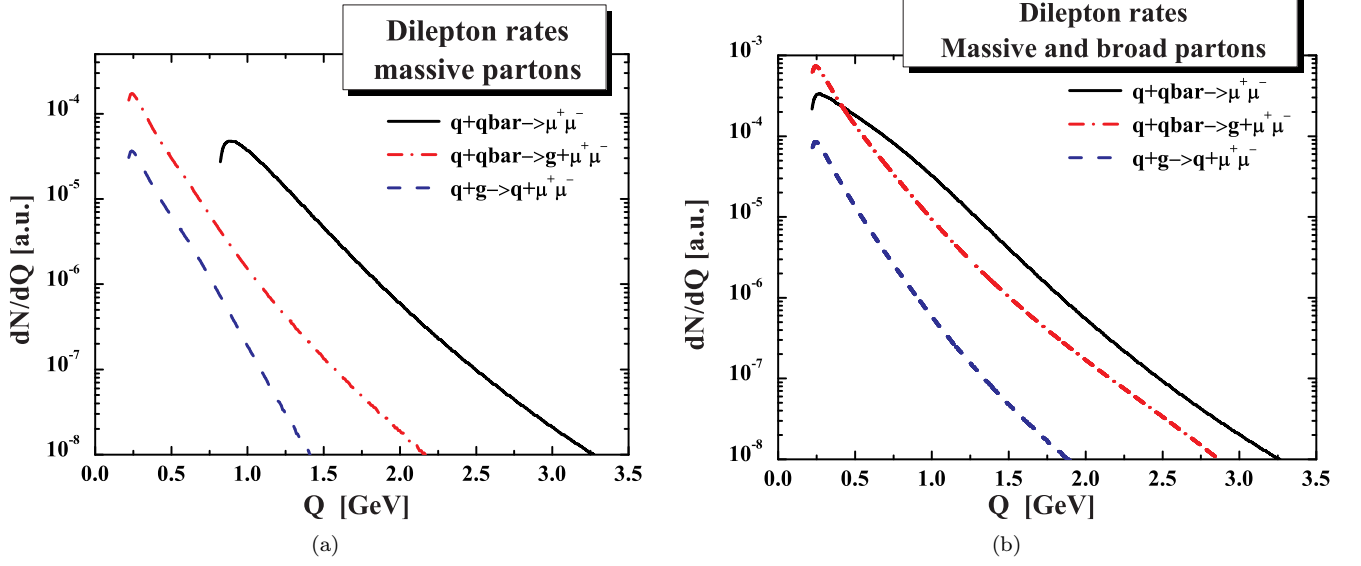


FIG. 12: (color online) Dimuon rates from QGP dN/dy beyond the on-shell approximation, $\alpha_S = 0.8$. **L.h.s.** dN/dQ calculated using the derived off-shell cross sections for quarks and gluons as massive quasi-particles, quark mass being set to $m_q = 0.3$ GeV and gluon mass to $\mu = 0.8$ GeV. Black solid line shows the contribution of the Drell-Yan channel ($q + \bar{q} \rightarrow \mu^+ \mu^-$), red dash-dotted line represents the contribution of the channel $q + \bar{q} \rightarrow g + \mu^+ \mu^-$, blue dashed line shows the contribution of the channel $q + g \rightarrow q + \mu^+ \mu^-$. **R.h.s.** dN/dQ calculated in the fully off-shell case of massive *and broad* dynamical quasi-particles. The rates are calculated using the derived off-shell cross sections and convoluted with effective spectral functions of the Breit-Wigner type. The parameters of the spectral functions are: the peak of the quark spectral function is located at 0.3 GeV, the width is $\Gamma = 0.3$ GeV, the peak of the gluon spectral function is at 0.8 GeV, the width to $\Gamma = 0.3$ GeV. Line coding is as on the l.h.s. The rates on both plots are in ‘arbitrary units’, reflecting our use of simplistic quark and gluon distributions in the QGP.

V. EFFECT OF THE FINAL QUARK AND GLUON WIDTH ON THE QGP RADIATION

Finally, we calculate the QGP dilepton rate, taking into account not only the finite masses of the partons, but also their *broad spectral functions*, i.e. finite widths. For this purpose, we convolute the off-shell cross sections obtained in section III with $dN/d\sqrt{s}$ and with the spectral functions $A(m)$ according to the equation (35).

The partonic spectral functions are related to the imaginary part of the trace of the effective propagator D_μ^μ and to the partonic self-energies Σ as follows:

$$\begin{aligned} A(p) &= \frac{1}{\pi} \Im D_\mu^\mu(p) \\ &= -\frac{1}{\pi} \frac{\Im \Sigma(p)}{[p^2 - m_{current}^2 - \text{Re} \Sigma(p)]^2 + [\Im \Sigma(p)]^2} \end{aligned} \quad (38)$$

For the current qualitative analysis, we use the approximation of constant real and imaginary parts of the self-energy, which corresponds to constant finite average mass for quarks ($\langle m_q \rangle$) and gluons (μ) and their width Γ . Within these approximations, the spectral function has the Breit-Wigner form.

The results of the numeric convolution of the off-shell cross sections with the spectral functions and the $dN/d\sqrt{s}$ are shown in Fig. 12(b) for realistic values of the spectral function parameters inspired by DQPM: the peak of the quark spectral function is located at 0.3 GeV,

the width is $\Gamma = 0.3$ GeV, the peak of the gluon spectral function is at 0.8 GeV, the width $\Gamma = 0.3$ GeV. The rate from the Drell-Yan mechanism is shown by solid black line, while for the $Q(\alpha_S) 2 \rightarrow 2$ processes by the dashed blue and dash-dotted red lines. We have checked numerically that the rates for different values of the gauge parameter lie on top of each other. For comparison, the rates shown on the l.h.s. of Fig. 12 have been obtained in the previous Section in the approximation of zero width (δ -functions for spectral functions).

By dressing the quark and gluon lines with effective spectral functions we model the effect of the quasi-particle interaction, including their multiple scattering. One observes by direct comparison of the l.h.s. and r.h.s. of the Fig. 12 that the effect on the dilepton rates is quite dramatic. In particular, the threshold of the Drell-Yan contribution is “washed-out”. In this observation we confirm the results of [51]. On the other hand, the effect of the partonic width and/or of multiple scattering on the $2 \rightarrow 2$ processes has not been studied so far. Whether the predicted shape of the dilepton spectrum in Fig. 12(b) is realized remains to be answered in the comparison to experimental data [76].

VI. SUMMARY AND OUTLOOK

In the present work, we have derived the off-shell cross sections of dilepton production by the constituents of the strongly interacting quark-gluon-plasma in the reactions $q + \bar{q} \rightarrow l^+l^-$ (Drell-Yan mechanism), $q + \bar{q} \rightarrow g + l^+l^-$ (quark annihilation with the gluon Bremsstrahlung in the final state), $q(\bar{q}) + g \rightarrow q(\bar{q}) + l^+l^-$ (gluon Compton scattering), $g \rightarrow q + \bar{q} + l^+l^-$ and $q(\bar{q}) \rightarrow q(\bar{q}) + g + l^+l^-$ (virtual gluon decay, virtual quark decay) by dressing the quark and gluon lines in the perturbative diagrams with effective non-perturbative propagators.

We show that finite quark and gluon virtualities modify the magnitude, Q and q_T dependence of the cross sections of all the calculated processes compared to the leading twist perturbative results for massless partons. The modification is higher at low Q^2 and on the edges of the phase space.

In QGP, quarks and gluons quasiparticles have broad spectral functions (due to large interaction rates), where the width encodes the effects of rescattering and gluon radiation. We have found that the finite width of partons has a dramatic effect on the dilepton rates in QGP, especially at low Q^2 . In particular, the threshold of the Born

term is smeared, while the contribution of the $2 \rightarrow 2$ processes to the rate is increased.

The cross sections obtained in this study will form the basis of a consistent calculation of the dilepton production in heavy ion collisions at SPS and RHIC energy by implementing the partonic processes into a transport approach of the PHSD collaboration [76]. The comparison to the dilepton data of the NA60 and PHENIX Collaborations double differentially in mass and p_T will open the possibility to study the relative importance of different processes in the dilepton production and guide us towards a better understanding of the properties of matter created in heavy-ion collisions.

Acknowledgements

The author acknowledges valuable discussions with E. Bratkovskaya, W. Cassing, J. Manninen, V. Begun and A. Toia and the financial support through the ‘‘HIC for FAIR’’ framework of the ‘‘LOEWE’’ program.

-
- [1] I. Tserruya, (2009), 0903.0415.
 - [2] R. J. Fries, B. Müller, and D. K. Srivastava, Phys. Rev. Lett. **90**, 132301 (2003).
 - [3] E. V. Shuryak, Sov. Phys. JETP **47**, 212 (1978).
 - [4] E. V. Shuryak, Phys. Lett. **B78**, 150 (1978), Sov.J.Nucl.Phys. **28** (1978) 408, Yad.Fiz. **28** (1978) 796.
 - [5] E. L. Feinberg, Izv. Akad. Nauk Ser. Fiz. **34**, 1987 (1970).
 - [6] E. L. Feinberg, Nuovo Cim. **A34**, 391 (1976).
 - [7] J. D. Bjorken and H. Weisberg, Phys. Rev. **D13**, 1405 (1976).
 - [8] NA60, R. Arnaldi *et al.*, Phys. Rev. Lett. **96**, 162302 (2006).
 - [9] NA60, J. Seixas *et al.*, J. Phys. **G34**, S1023 (2007).
 - [10] NA60, S. Damjanovic *et al.*, Nucl. Phys. **A783**, 327 (2007).
 - [11] R. Rapp, J. Wambach, and H. van Hees, (2009), 0901.3289.
 - [12] O. Linnyk, E. L. Bratkovskaya, and W. Cassing, Nucl. Phys. **A830**, 491c (2009).
 - [13] O. Linnyk, E. L. Bratkovskaya, and W. Cassing, (2010), 1001.3858.
 - [14] W. Cassing and E. L. Bratkovskaya, Phys. Rept. **308**, 65 (1999).
 - [15] E. L. Bratkovskaya, W. Cassing, and O. Linnyk, Phys. Lett. **B670**, 428 (2009).
 - [16] PHENIX, A. Toia, Nucl. Phys. **A774**, 743 (2006).
 - [17] PHENIX, A. Toia, Eur. Phys. J. **C49**, 243 (2007).
 - [18] PHENIX, S. Afanasiev *et al.*, (2007), 0706.3034.
 - [19] PHENIX, A. Adare *et al.*, (2009), 0912.0244.
 - [20] F. Halzen and D. M. Scott, Phys. Rev. **D18**, 3378 (1978).
 - [21] Z.-w. Lin and C. M. Ko, Nucl. Phys. **A671**, 567 (2000).
 - [22] L. D. McLerran and T. Toimela, Phys. Rev. **D31**, 545 (1985).
 - [23] E. Shuryak, Prog. Part. Nucl. Phys. **53**, 273 (2004).
 - [24] M. H. Thoma, J. Phys. **G31**, L7 (2005).
 - [25] A. Peshier and W. Cassing, Phys. Rev. Lett. **94**, 172301 (2005).
 - [26] PHENIX, K. Adcox *et al.*, Nucl. Phys. **A757**, 184 (2005).
 - [27] STAR, J. Adams *et al.*, Nucl. Phys. **A757**, 102 (2005).
 - [28] BRAHMS, I. Arsene *et al.*, Nucl. Phys. **A757**, 1 (2005).
 - [29] PHOBOS, B. B. Back *et al.*, Nucl. Phys. **A757**, 28 (2005).
 - [30] F. Karsch, Nucl. Phys. **A698**, 199 (2002).
 - [31] F. Halzen and D. M. Scott, Phys. Rev. Lett. **40**, 1117 (1978).
 - [32] J. I. Kapusta, P. Lichard, and D. Seibert, Phys. Rev. **D44**, 2774 (1991).
 - [33] E. Braaten, R. D. Pisarski, and T.-C. Yuan, Phys. Rev. Lett. **64**, 2242 (1990).
 - [34] S. M. H. Wong, Z. Phys. **C58**, 159 (1993).
 - [35] R. D. Pisarski, Phys. Rev. Lett. **63**, 1129 (1989).
 - [36] V. P. Silin, Sov. Phys. J.E.T.P. **11**, 1136 (1960).
 - [37] V. V. Klimov, Sov. Phys. J.E.T.P. **55**, 199 (1982).
 - [38] H. A. Weldon, Phys. Rev. **D26**, 1394 (1982).
 - [39] R. Baier, M. Dirks, and K. Redlich, Acta Phys. Polon. **B28**, 2873 (1997).
 - [40] M. Strickland, Phys. Lett. **B331**, 245 (1994).
 - [41] J.-P. Blaizot and F. Gelis, Eur. Phys. J. **C43**, 375 (2005).
 - [42] F. Gelis, Nucl. Phys. **A715**, 329 (2003).
 - [43] W. Cassing, Nucl. Phys. **A795**, 70 (2007).
 - [44] A. Peshier, B. Kämpfer, O. P. Pavlenko, and G. Soff, Phys. Lett. **B337**, 235 (1994).
 - [45] M. H. Thoma, S. Leupold, and U. Mosel, Eur. Phys. J. **A7**, 219 (2000).
 - [46] F. Karsch, E. Laermann, P. Petreczky, S. Stickan, and I. Wetzorke, Phys.Lett. **B530**, 147 (2002).

- [47] M. I. Gorenstein and O. A. Mogilevsky, Phys. Lett. **B228**, 121 (1989).
- [48] L. D. Landau and I. Pomeranchuk, Dokl. Akad. Nauk Ser. Fiz. **92**, 535 (1953).
- [49] L. D. Landau and I. Pomeranchuk, Dokl. Akad. Nauk Ser. Fiz. **92**, 735 (1953).
- [50] A. B. Migdal, Phys. Rev. **103**, 1811 (1956).
- [51] P. Aurenche, F. Gelis, G. D. Moore, and H. Zaraket, JHEP **12**, 006 (2002).
- [52] W. Cassing, Nucl. Phys. **A791**, 365 (2007).
- [53] O. Linnyk, S. Leupold, and U. Mosel, Phys. Rev. **D75**, 014016 (2007).
- [54] E. V. Shuryak and A. I. Vainshtein, Nucl. Phys. **B199**, 451 (1982).
- [55] M. Gluck, E. Reya, and A. Vogt, Eur. Phys. J. **C5**, 461 (1998).
- [56] W. J. Stirling and M. R. Whalley, J. Phys. **G19**, D1 (1993).
- [57] R. Hamberg, W. L. van Neerven, and T. Matsuura, Nucl. Phys. **B359**, 343 (1991), Erratum - ibid. **B644** (2002) 403.
- [58] R. K. Ellis, W. J. Stirling, and B. R. Webber, *QCD and collider physics* (Camb. Monogr. Part. Phys. Nucl. Phys. Cosmol. **8**, 1996).
- [59] J. Collins and H. Jung, (2005), hep-ph/0508280.
- [60] O. Linnyk, S. Leupold, and U. Mosel, Phys. Rev. **D71**, 034009 (2005).
- [61] E. L. Bratkovskaya, S. M. Kiselev, and G. B. Sharkov, Phys. Rev. **C78**, 034905 (2008).
- [62] R. L. Jaffe, Lectures presented at the Los Alamos School on Quark Nuclear Physics, Los Alamos, N.Mex., Jun 10-14, 1985.
- [63] S. D. Drell and T.-M. Yan, Phys. Rev. Lett. **24**, 181 (1970).
- [64] G. Altarelli, G. Parisi, and R. Petronzio, Phys. Lett. **B76**, 351 (1978).
- [65] A. I. Vainshtein, V. I. Zakharov, V. A. Novikov, and M. A. Shifman, JETP Lett. **24**, 341 (1976), [Pisma Zh. Eksp. Teor. Fiz. **24**, 376 (1976)].
- [66] M. E. Peskin and D. V. Schroeder, *An Introduction to quantum field theory* (Reading, USA: Addison-Wesley, 1995).
- [67] A. H. Compton, Phys. Rev. **21**, 483 (1923).
- [68] A. H. Compton, Phys. Rev. **22**, 409 (1923).
- [69] J. C. Webb, (2003), hep-ex/0301031.
- [70] A. I. Akhiezer and V. B. Berestetsky, *Quantum electrodynamics (in Russian)* (Moscow: Nauka, 1981).
- [71] T. H. West, Comp. Phys. Comm. **77**, 286 (1993).
- [72] S. Wolfram, *The Mathematica Book, Fifth Edition* (Champaign, USA: Wolfram Media, 2003).
- [73] F. Karsch, E. Laermann, and A. Peikert, Phys. Lett. **B478**, 447 (2000).
- [74] V. V. Begun, M. I. Gorenstein, and O. A. Mogilevsky, (2010), 1001.3139.
- [75] O. Linnyk, E. L. Bratkovskaya, and W. Cassing, Int. J. Mod. Phys. **E17**, 1367 (2008).
- [76] O. Linnyk, E. L. Bratkovskaya, and W. Cassing, *work in progress*.
- [77] The absolute magnitudes of the dilepton rates presented in Figs.10,14,15 and 16 are not to be directly compared to experimental data. The analysis of the relative yields serves as an illustration of an application of the derived off-shell cross sections.

